Signal intensity informed multi-coil encoding operator for physics-guided deep learning reconstruction of highly accelerated myocardial perfusion CMR

Demirel, Omer Burak; Yaman, Burhaneddin; Shenoy, Chetan; Moeller, Steen; Weingärtner, Sebastian; Akçakaya, Mehmet

DOI
10.1002/mrm.29453

Publication date
2022

Document Version
Final published version

Published in
Magnetic Resonance in Medicine

Received: 22 February 2022 | Revised: 21 July 2022 | Accepted: 21 August 2022

DOI: 10.1002/mrm.29453

Magnetic Resonance in Medicine

TECHNICAL NOTE

Signal intensity informed multi-coil encoding operator for physics-guided deep learning reconstruction of highly accelerated myocardial perfusion CMR

Omer Burak Demirel[1,2] | **Burhaneddin Yaman**[1,2] | **Chetan Shenoy**[3] | **Steen Moeller**[2] | **Sebastian Weingärtner**[4] | **Mehmet Akçakaya**[1,2]

[1]Department of Electrical and Computer Engineering, University of Minnesota, Minneapolis, Minnesota, USA

[2]Center for Magnetic Resonance Research, University of Minnesota, Minneapolis, Minnesota, USA

[3]Department of Medicine (Cardiology), University of Minnesota, Minneapolis, Minnesota, USA

[4]Department of Imaging Physics, Delft University of Technology, Delft, Netherlands

Correspondence
Mehmet Akçakaya, University of Minnesota, 200 Union Street S.E., Minneapolis, MN, 55455, USA.
Email: akcakaya@umn.edu

Funding information
4TU Federation; American Heart Association, Grant/Award Number: Predoctoral Fellowship; Health Technology Programme TU Delft - LUMC; National Heart, Lung, and Blood Institute, Grant/Award Number: R01HL153146; National Institute of Biomedical Imaging and Bioengineering, Grant/Award Numbers: P41EB027061, R21EB028369; National Science Foundation, Grant/Award Number: CAREER CCF-1651825; Stichting voor de Technische Wetenschappen, Grant/Award Number: STU.019.024

Purpose: To develop a physics-guided deep learning (PG-DL) reconstruction strategy based on a signal intensity informed multi-coil (SIIM) encoding operator for highly-accelerated simultaneous multislice (SMS) myocardial perfusion cardiac MRI (CMR).

Methods: First-pass perfusion CMR acquires highly-accelerated images with dynamically varying signal intensity/SNR following the administration of a gadolinium-based contrast agent. Thus, using PG-DL reconstruction with a conventional multi-coil encoding operator leads to analogous signal intensity variations across different time-frames at the network output, creating difficulties in generalization for varying SNR levels. We propose to use a SIIM encoding operator to capture the signal intensity/SNR variations across time-frames in a reformulated encoding operator. This leads to a more uniform/flat contrast at the output of the PG-DL network, facilitating generalizability across time-frames. PG-DL reconstruction with the proposed SIIM encoding operator is compared to PG-DL with conventional encoding operator, split slice-GRAPPA, locally low-rank (LLR) regularized reconstruction, low-rank plus sparse (L + S) reconstruction, and regularized ROCK-SPIRiT.

Results: Results on highly accelerated free-breathing first pass myocardial perfusion CMR at three-fold SMS and four-fold in-plane acceleration show that the proposed method improves upon the reconstruction methods use for comparison. Substantial noise reduction is achieved compared to split slice-GRAPPA, and aliasing artifacts reduction compared to LLR regularized reconstruction, L + S reconstruction and PG-DL with conventional encoding. Furthermore, a qualitative reader study indicated that proposed method outperformed all methods.

Conclusion: PG-DL reconstruction with the proposed SIIM encoding operator improves generalization across different time-frames /SNRs in highly accelerated perfusion CMR.

KEYWORDS

accelerated imaging, cardiac MRI, coil maps, deep learning, image reconstruction, myocardial perfusion

1 | INTRODUCTION

Myocardial perfusion cardiac MRI (CMR) is used for functional assessment of stenoses in diagnosing coronary artery disease.[1–7] Clinically, myocardial perfusion CMR is acquired using snap-shot imaging during the first pass of an exogenous contrast agent, which results in limited resolution and coverage.[8–10] Low spatial resolution has been associated with dark rim artifacts that can compromise assessment of perfusion abnormalities.[11] Additionally, coverage is typically limited to three to four non-contiguous slices,[12] which may result in missed regions in microvascular disease. Furthermore, limited temporal resolution is associated with low contrast-to-noise ratios and may produce cardiac motion artifacts.[13] Therefore, trade-offs between spatio-temporal resolution and coverage still remain a major challenge in myocardial perfusion CMR, necessitating accelerated imaging techniques.

Parallel imaging has long been used in perfusion CMR but is limited to two- to three-fold acceleration.[12] Spatio-temporal reconstruction (k-t) methods[14–16] have been proposed, but their acceleration rates remained limited.[17] Subsequently, compressed sensing, low-rank methods, and their combinations have been adopted to perfusion CMR reconstruction to enable higher acceleration rates.[18–40] These have enabled 3D whole heart myocardial perfusion,[41–49] although a recent study has shown that 2D high resolution scans with smaller temporal footprint are more sensitive for detecting ischemia.[50] Recently, simultaneous multislice (SMS) imaging has gained interest in CMR for improved coverage with minimal loss in image quality and SNR.[21,23,51–54] Yet, ultra-high acceleration rates are still limited when SMS imaging is combined with in-plane acceleration due to noise amplification.[55]

Physics-guided deep learning (PG-DL) techniques have recently gained substantial interest in accelerated MRI, showing improved reconstruction quality at high acceleration rates compared to parallel imaging or compressed sensing.[56–63] These PG-DL techniques use a forward encoding operator incorporating MRI physics, while the proximal operation associated with regularization is solved implicitly by neural networks.[61] However, PG-DL networks have several challenges that hamper their applicability in perfusion CMR. A 2D implementation processing slices/time-frames individually is a natural choice from an implementation perspective, and for avoiding temporal blurring. However, signal intensity changes across time-frames hinder the utility of such PG-DL networks, which have exhibited generalizability issues with such variations.[64] An alternative way to train PG-DL reconstruction for perfusion CMR would be using a spatio-temporal network, yet this has its own challenges including memory limitations[65] and difficulty of procuring high-quality training databases due to differences in contrast uptakes/breathing patterns among subjects. Thus, application of PG-DL reconstruction to perfusion CMR has been difficult, and existing DL methods for perfusion CMR reconstruction have been limited to data-driven image enhancement networks,[66–68] which are trained in a supervised manner using conventional compressed sensing reconstruction outputs as reference images. While this line of work improves reconstruction speed, the reconstruction quality is inherently limited by the conventional reconstruction used as reference for supervised training, which in turn hinders the true potential of DL reconstruction for perfusion CMR.

In this study, we propose to use a signal intensity informed multi-coil (SIIM) encoding operator in PG-DL networks to improve highly accelerated perfusion CMR reconstruction. The proposed SIIM encoding operator is inherently aware of contrast/SNR changes across time-frames, leading to a uniform/flat signal level at the output of the network, which in turn assists the generalizability of PG-DL methods. Proposed SIIM encoding operator was compared with PG-DL using conventional operator, and conventional reconstruction methods, including split slice-GRAPPA,[69] locally low-rank (LLR) regularization,[34,70] regularized ROCK-SPIRIT[71] and a low-rank plus sparse (L + S) reconstruction[35] for free-breathing first-pass perfusion with three-fold SMS and four-fold in-plane acceleration. Results show that PG-DL reconstruction with the proposed SIIM encoding operator improves upon the other methods by reducing noise and residual artifacts.

2 | METHODS

2.1 | PGDL reconstruction

The inverse problem for MRI reconstruction is formulated as an optimization problem

$$\hat{\mathbf{x}}_{\text{reg}} = \arg\min_{\mathbf{x}} \left\| \mathbf{y}_{\Omega} - \mathbf{E}_{\Omega}\boldsymbol{x} \right\|_2^2 + \mathcal{R}(\mathbf{x}), \tag{1}$$

where $\mathbf{y}_{\Omega}$ is the acquired multi-channel k-space, Ω is the in-plane undersampling pattern, $\mathbf{E}_{\Omega}$ is the multi-coil encoding operator, $\mathbf{x}$ is the image of interest, and $\mathbf{n}$ is measurement noise. At high acceleration rates, this system is typically ill-conditioned. The first quadratic term enforces the data fidelity (DF) with acquired k-space points, and the second term $\mathcal{R}(\cdot)$ is a regularizer. This objective function may be solved using a multitude of techniques,[72] which decouple the DF and regularizer terms into a series of sub-problems, including variable splitting with quadratic penalty,[61] described in detail in Supporting Information Figure S1, which is available online.

2.2 | Conventional multi-coil encoding operator

The encoding operator $\mathbf{E}_\Omega$ in Eq. [1] is given as:

$$\mathbf{E}_\Omega = \begin{bmatrix} \mathbf{F}_\Omega \mathbf{S}_1 \\ \vdots \\ \mathbf{F}_\Omega \mathbf{S}_C \end{bmatrix},$$

where $\mathbf{F}_\Omega$ is a sub-sampled Fourier operator sampling the k-space locations specified by Ω, and $\mathbf{S}_c$ is a diagonal matrix representing the c^{th} coil sensitivity map. In practice, $\mathbf{S}_c$ are estimated via ESPIRiT,[73] and inherently encode B_1^-, which remain fixed across time-frames. Therefore, the solution of Eq. [1] presents varying signal intensities across time-frames, which mirror SNR variations in acquired k-space across time-frames.

2.3 | SIIM encoding operator

We propose to encode dynamically-varying signal intensity in the encoding operator for PG-DL reconstruction. Let $\mathbf{L}$ be a diagonal matrix whose entries are the pixel values of an image that contains the signal intensity information of a given time-frame. We define the SIIM encoding operator as:

$$\mathbf{H}_\Omega = \mathbf{E}_\Omega \cdot \mathbf{L}, \tag{3}$$

where the inherent signal intensity variation across time-frames is encoded into encoding operator via $\mathbf{L}$. Note that for perfusion CMR, we indeed have multiple $\mathbf{L}^t, t \in \{1, \cdots, T\}$ where T is the number of time-frames, but for ease of notation, we use $\mathbf{L}$ for a given time-frame of interest. Consequently, the inverse problem for SIIM encoding operator is:

$$\hat{\mathbf{x}}_{\text{SIIM}} = \arg\min_{\mathbf{x}} \left\| \mathbf{y}_\Omega - \mathbf{H}_\Omega \mathbf{x} \right\|_2^2 + \mathcal{R}(\mathbf{x}). \tag{4}$$

In the absence of a regularizer, it is easy to show[74]

$$\begin{aligned} \hat{\mathbf{x}}_{\text{reg}} &= \left(\mathbf{E}_\Omega^* \mathbf{E}_\Omega\right)^{-1} \mathbf{E}_\Omega^* \mathbf{y}_\Omega \\ &= \left(\left(\mathbf{L}^{-1}\right)^* \mathbf{H}_\Omega^* \mathbf{H}_\Omega \mathbf{L}^{-1}\right)^{-1} \left(\mathbf{L}^{-1}\right)^* \mathbf{H}_\Omega^* \mathbf{y}_\Omega \\ &= \mathbf{L}\left(\mathbf{H}_\Omega^* \mathbf{H}_\Omega\right)^{-1} \mathbf{H}_\Omega^* \mathbf{y}_\Omega \\ &= \mathbf{L} \cdot \hat{\mathbf{x}}_{\text{SIIM}}, \end{aligned} \tag{5}$$

where * is the Hermitian transpose. Thus, the underlying signal intensity information is restored by multiplication with the corresponding signal intensity informed images.

Signal intensity variations for a given time-frame can be captured with a low-resolution image, generated from central k-space, as the diagonal entries of $\mathbf{L}$. In the context of parallel imaging, a similar concept was used, where low-resolution images from central k-space were used as coil maps, without normalizing them by their root-sum-squares image,[74] and the signal intensity information was restored by multiplication with the root-sum-squares image, as in Eq. [5]. In this work, we instead use the formulation in Eq. [3], since this enables a more synergistic combination with ESPIRiT map estimation.

There are two major differences between SIIM and conventional encoding operators. First, there are numerical differences in solving the objective functions in Eqs. [1] and [4], which was also noted for the unregularized case in parallel imaging.[74] Thus, the SIIM formulation may overcome numerical instabilities at high acceleration rates. Second, in the regularized setup, the SIIM encoding operator has the additional benefit that the solutions of Eq. [4] have more uniform/flat signal intensity across time-frames of varying SNR, as depicted in Figure 1A. This in turn assists the regularizer to work with consistent signal intensity regardless of the physiological process associated with a time-frame. Hence, the use of the SIIM operator may lead to improved generalizability for PG-DL reconstructions, which have been shown to be affected by SNR variations of the underlying solutions. Schematics of unrolled networks using conventional and proposed SIIM encoding operators are shown in Figure 1B.

2.4 | Imaging experiments

Free-breathing first-pass myocardial perfusion CMR was acquired on a 3T Siemens Magnetom Prisma (Siemens Healthineers) in eight subjects (six men, two women, age:39 ± 18 y). This study was approved by our institutional review board, and written informed consent was obtained before each examination. A saturation-prepared GRE sequence was used, with relevant imaging parameters: FOV = $360 \times 320\,\text{mm}^2$; spatial resolution = $1.7 \times 1.7\,\text{mm}^2$; slice thickness = 8 mm; temporal resolution = 116 ms; SMS factor = 3 (1/3 FOV shifts with CAIPIRINHA [75]); in-plane acceleration = 4 (uniform undersampling, no ACS) and partial Fourier = 6/8 (overall 16-fold acceleration).[55] Non-prepared GRE calibration scans were acquired at a lower spatial resolution = $1.7 \times 5.6\,\text{mm}^2$ individually for all 9 slices. Details of the imaging sequence are given in Supporting Information Table S1.

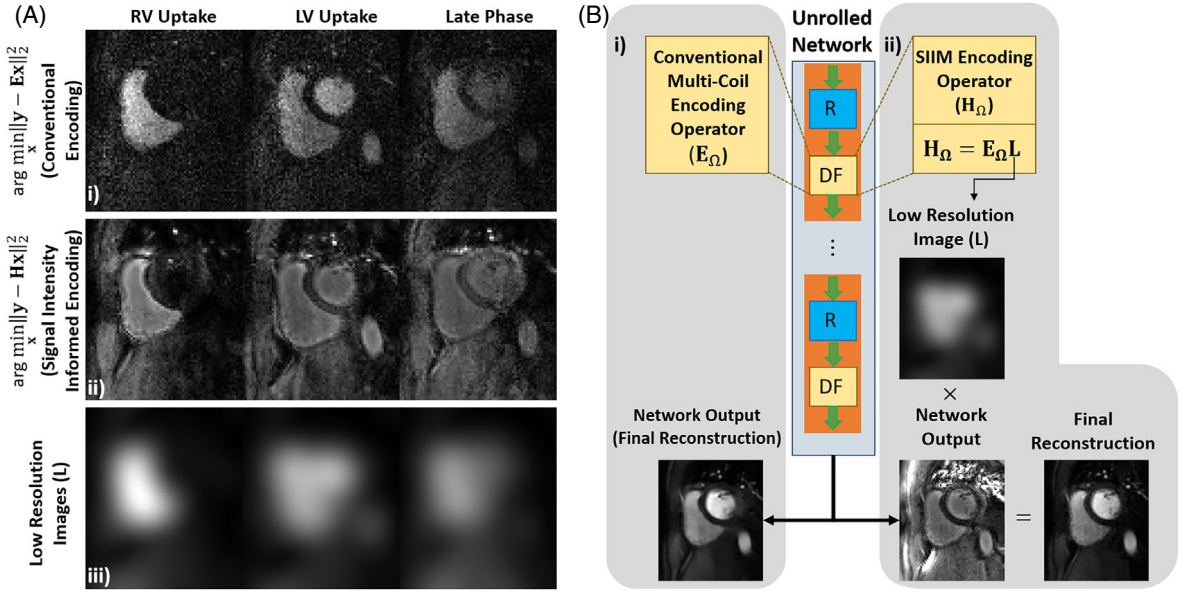

FIGURE 1 (A), Unregularized least squares estimate of a representative slice using: (i) conventional encoding and (ii) proposed SIIM encoding operator. Signal intensity changes are visible across time-frames in (i). A more uniform/flat signal level is observed across time-frames using proposed SIIM encoding operator in (ii). (iii) Corresponding low-resolution images (L) for the slice of interest for right ventricular uptake (RV), left ventricular uptake (LV), and a late phase are shown. The product of middle and bottom rows yields similar contrast to top row, as given in Eq. [9]. (B), A schematic of PG-DL reconstruction network with (i) conventional multi-coil encoding operator using ESPIRiT maps and (ii) proposed SIIM encoding operator. The network outputs are different between the two encoding operators, with the latter showing a flatter signal intensity. The product of the network output for the SIIM operator with low resolution images (L) yields similar contrast to the network output for the conventional operator.

2.5 | SIIM encoding operator formation

Coil maps ($\mathbf{S}_C$) were generated via ESPIRiT using central 24×24 regions of the calibrations scans of the corresponding slices.[73] Low-resolution images ($\mathbf{L}$) for each time-frame and slice were generated from the central 24×24 k-space region reconstructed using split slice-GRAPPA.[69] Note that this intermediate reconstruction step was necessary due to the lack of individual k-spaces for the slices of individual time-frames resulting from SMS encoding, and would not be necessary for single-slice/volume imaging. Subsequently, a Blackman filter was applied for ringing,[76] followed by taking the magnitude of the SENSE-1 combination of individual coil images.[77] Finally, SIIM encoding operator $\mathbf{H}_\Omega$ was generated by multiplying $\mathbf{E}_\Omega$ by $\mathbf{L}$, whose diagonal entries were the intensity values of the aforementioned magnitude SENSE-1 image, as in Eq. [3]. Further implementation details for SMS encoding are provided in Supporting Information Figure S2.

2.6 | Network and training details

Due to lack of fully-sampled reference data in this highly accelerated SMS perfusion CMR acquisition, the recently proposed self-supervised learning via data undersampling (SSDU) was used for training.[61,78,79] Details of the multi-mask version of SSDU[80] are given in Supporting Information Figure S3. PG-DL training with multi-mask SSDU was performed on 4 subjects using the last 35 time-frames out of 40, for all three sets of SMS acquisitions per subject for a total number of 420 SMS-encoded k-spaces. Training and network details are provided in Supporting Information Table S2 and Figure S4. Two separate trainings were performed using the same network architecture, one with conventional and other with proposed SIIM encoding operator. Implementation of the proposed method will be provided online (https://imagine.umn.edu/research/software).

Testing was performed on 4 different subjects not used in training. Outputs of PG-DL network with SIIM encoding were multiplied with the corresponding low-resolution images ($\boldsymbol{L}$) as shown in Figure 1B to restore the underlying signal intensity. Comparisons were made to split slice-GRAPPA, LLR regularized reconstruction, L + S reconstruction and regularized ROCK-SPIRiT, whose hyperparameters were tuned empirically. Further implementation details are provided in Supporting Information Table S3.

Additionally, a numerical perfusion phantom[81] was used to evaluate the performance of different

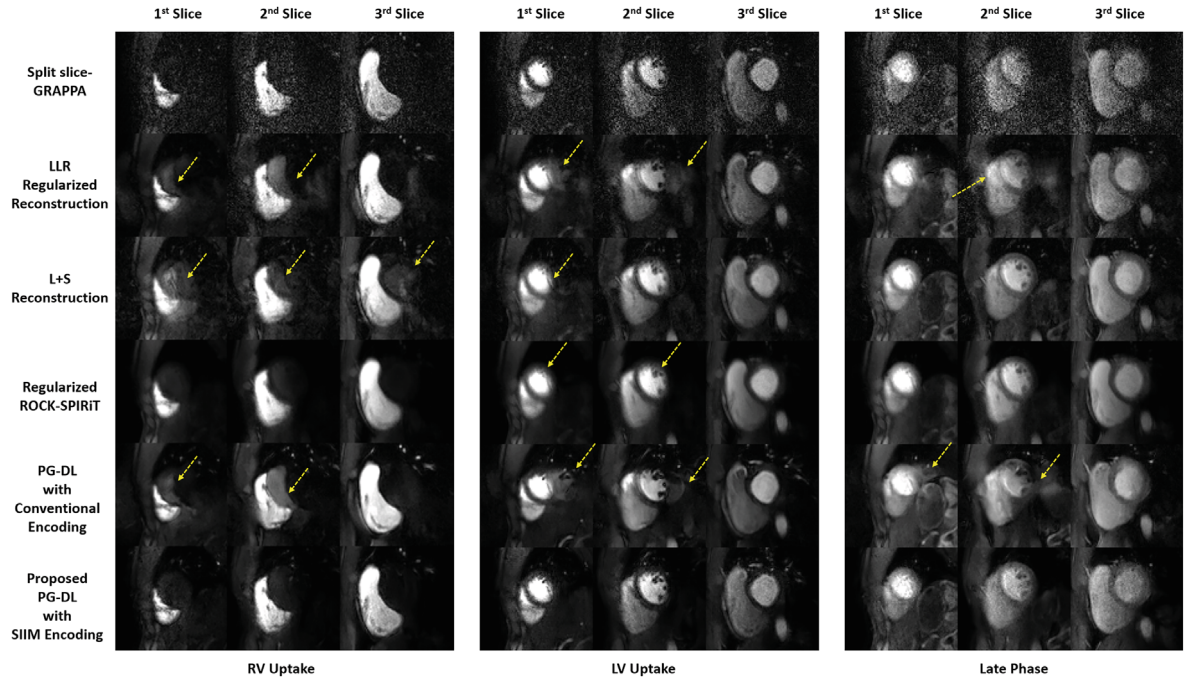

FIGURE 2 Representative perfusion CMR results across three different time-frames on a test subject, acquired with a 3-fold SMS and 4-fold in-plane acceleration along with 6/8 partial Fourier (overall 16-fold acceleration). Split slice-GRAPPA (top row) shows aliasing-free reconstruction albeit at substantial noise amplification, while LLR-regularized reconstruction (second row) and L + S reconstruction (third row) reduce the noise but suffer from aliasing artifacts (yellow arrows). Regularized ROCK-SPIRiT (fourth row) and PG-DL with conventional encoding (fifth row) also show reduced noise albeit with blurring and aliasing artifacts (yellow arrows), respectively. Proposed PG-DL reconstruction with SIIM encoding operator (bottom row) improves upon all techniques showing higher image quality by suppressing noise amplification and aliasing artifacts.

reconstruction methods, using in-vivo trained models. The details and results of these numerical experiments are presented in Supporting Information Tables S4 and S5 and Figures S5 and S7.

2.7 | Image analysis

Qualitative image quality assessment was performed by an experienced cardiologist (15 y of experience). The reader was blinded to the reconstruction methods, orders of which were randomized. Four test subjects (nine slices, all dynamics) were evaluated on a 4-point ordinal scale, for overall image quality (1:excellent; 2:good; 3:fair; 4:poor), blurring (1:none; 2:mild; 3:moderate; 4:severe) and perceived SNR (1:high SNR; 2:minor noise with moderate SNR; 3:major noise but not limiting clinical diagnosis; 4:poor SNR and nondiagnostic). Wilcoxon signed-rank test was used to evaluate the scores with a significance level of $P < 0.05$.

3 | RESULTS

Figure 2 shows reconstructed slices from an SMS slice group for right and left ventricular (RV/LV) uptakes, and a late phase, representing three different signal intensities/SNRs. Split slice-GRAPPA has no residual aliasing but suffers from high noise amplification especially in late phases with depleted SNR. LLR-regularized and L + S reconstructions reduce noise amplification, but exhibit residual aliasing artifacts. ROCK-SPIRiT also reduces noise but suffers from blurring during LV uptake. PG-DL with conventional encoding operator using ESPIRiT maps has reduced noise, but visible aliasing and inter-slice leakage. Regularized PG-DL with proposed SIIM encoding successfully removes aliasing and reduces noise, leading to improved image quality. Difference images between various reconstructions and linear baseline reconstruction split slice-GRAPPA are depicted in Supporting Information Figure S8. Proposed method shows noise-like differences with respect to split slice-GRAPPA, whereas residual artifacts are seen in all other regularized reconstructions. Videos of two subjects are included in Supporting Information Videos S1–S2.

Figure 3 depicts five slices from a different subject, with all nine slices depicted in Supporting Information Figure S9. Split slice-GRAPPA shows noise amplification throughout the heart. LLR-regularized reconstruction, L + S reconstruction and PG-DL with conventional encoding show reduced noise but visible residual artifacts, while

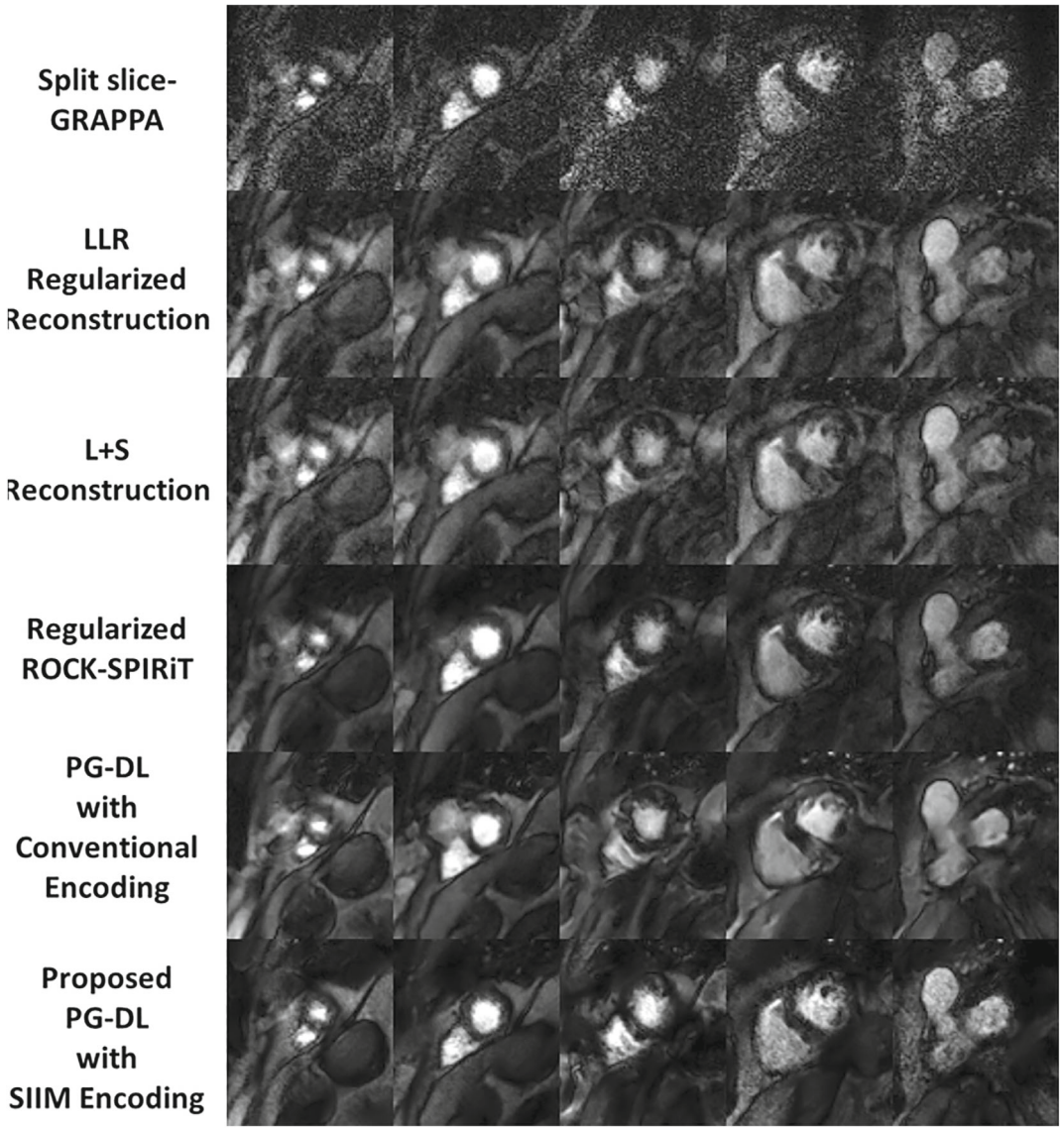

FIGURE 3 Reconstructions across five slices for a representative time-frame from another subject. Split slice-GRAPPA (top row) shows noise amplification across the heart, while LLR-regularized reconstruction (second row) and L + S reconstruction (third row) have visible residual aliasing artifacts lowering the image quality. On the other hand, regularized ROCK-SPIRiT (fourth row) shows blurring, and PG-DL with conventional encoding (fifth row) has visible residual aliasing artifacts especially in the myocardium. Proposed PG-DL with SIIM encoding operator (bottom row) shows improved image quality with reduced noise and no residual artifacts, as well as a clear delineation of the blood-myocardium interface. All nine slices using three SMS groups covering the whole heart is depicted in Supporting Information Figure S10.

regularized ROCK-SPIRiT shows blurring. PG-DL with SIIM encoding eliminates residual aliasing while reducing noise amplification, showing better image quality.

Figure 4A shows different time-frames of a slice. Dominant noise amplification is seen with split slice-GRAPPA, but without residual aliasing. LLR-regularized reconstruction, L + S reconstruction and PG-DL with conventional encoding reduce noise, but suffer from residual inter-slice aliasing. Similarly regularized ROCK-SPIRiT shows reduced noise, but exhibits blurring in LV uptake and aliasing in earlier time-frames. PG-DL with SIIM encoding shows improved image quality, suppressing noise and aliasing artifacts. Figure 4B,C show low-pass filtered[82] signal intensity curves in the LV blood pool and septal myocardium, averaged over respective ROIs. Split-slice GRAPPA and proposed method show good temporal agreement in myocardial uptake, with differences only prior to contrast injection, where split-slice GRAPPA exhibits a higher noise floor in the low SNR regime, as expected. The other reconstructions show misestimation of the uptake curve due to residual and blurring artifacts, consistent with earlier results. Myocardial signal

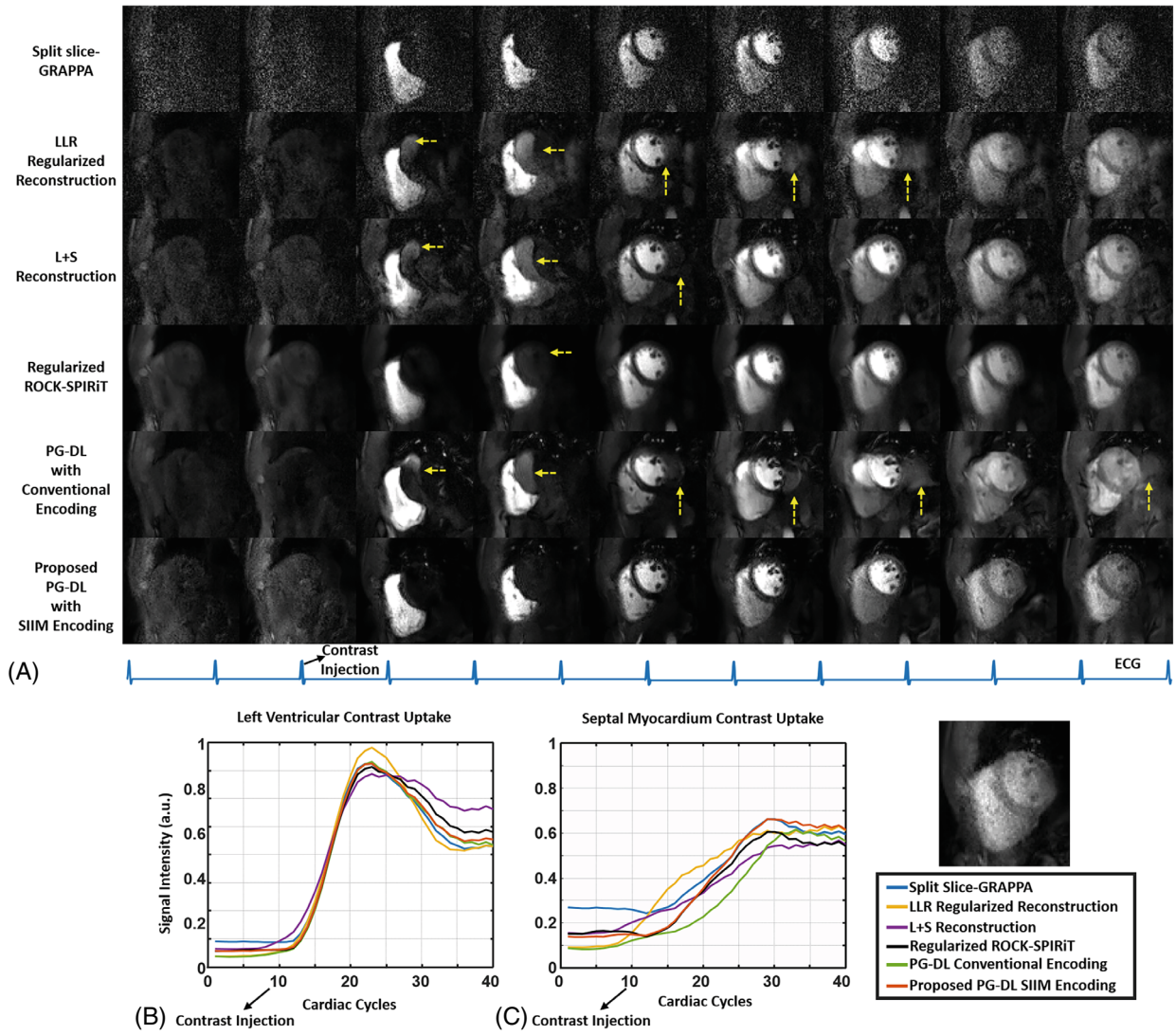

FIGURE 4 (A), Different time-frames of a slice of a perfusion CMR scan reconstructed with the different reconstruction methods. Dominant noise amplification is seen across all time-frames with split slice-GRAPPA, although no residual aliasing is observed. LLR-regularized reconstruction, L + S reconstruction and PG-DL with conventional encoding reduce noise, but suffer from residual inter-slice aliasing across time-frames. ROCK-SPIRiT shows reduced noise with aliasing artifacts in the earlier time-frames with blurring, especially in left-ventricular uptake. PG-DL with SIIM encoding operator shows improved image quality upon all methods, suppressing noise and aliasing artifacts, while maintaining a good image quality. (B), Low-pass filtered signal intensity curves in the left ventricular blood pool averaged over an ROI in one subject. Split slice-GRAPPA, regularized ROCK-SPIRiT, and proposed PG-DL with SIIM encoding operator show good temporal agreements during contrast uptake, where the averaging across pixels in the ROI reduces the overall effect of noise amplification in the split-slice GRAPPA curves. (C), Low-pass filtered signal intensity curves averaged in an ROI in septal myocardium. Split-slice GRAPPA and proposed PG-DL with SIIM encoding operator show good temporal agreement in the myocardium uptake curve. The only major differences are observed in the part of the curve prior to contrast injection, where split-slice GRAPPA exhibits a higher noise floor in the low SNR regime, as expected. On the other hand, PG-DL with conventional operator, LLR-regularized reconstruction and L + S reconstruction show severe misestimation of the uptake curve with respect to these two techniques due to dominant residual artifacts in the myocardium. Although regularized ROCK-SPIRiT follows proposed PG-DL with SIIM encoding operator during the first half of the time-frames, it drifts away in later phases due to blurring that distorts the myocardium blood-interface.

intensity curves for six AHA sectors are shown in Supporting Information Figure S10.

Figure 5 summarizes the reader study. Proposed PG-DL with SIIM encoding operator shows the best overall image quality among the methods, significantly improving on split slice-GRAPPA, LLR-regularized reconstruction, L + S reconstruction and PG-DL with conventional encoding. Similarly, the proposed method shows the least amount of blurring and highest perceived SNR among all methods.

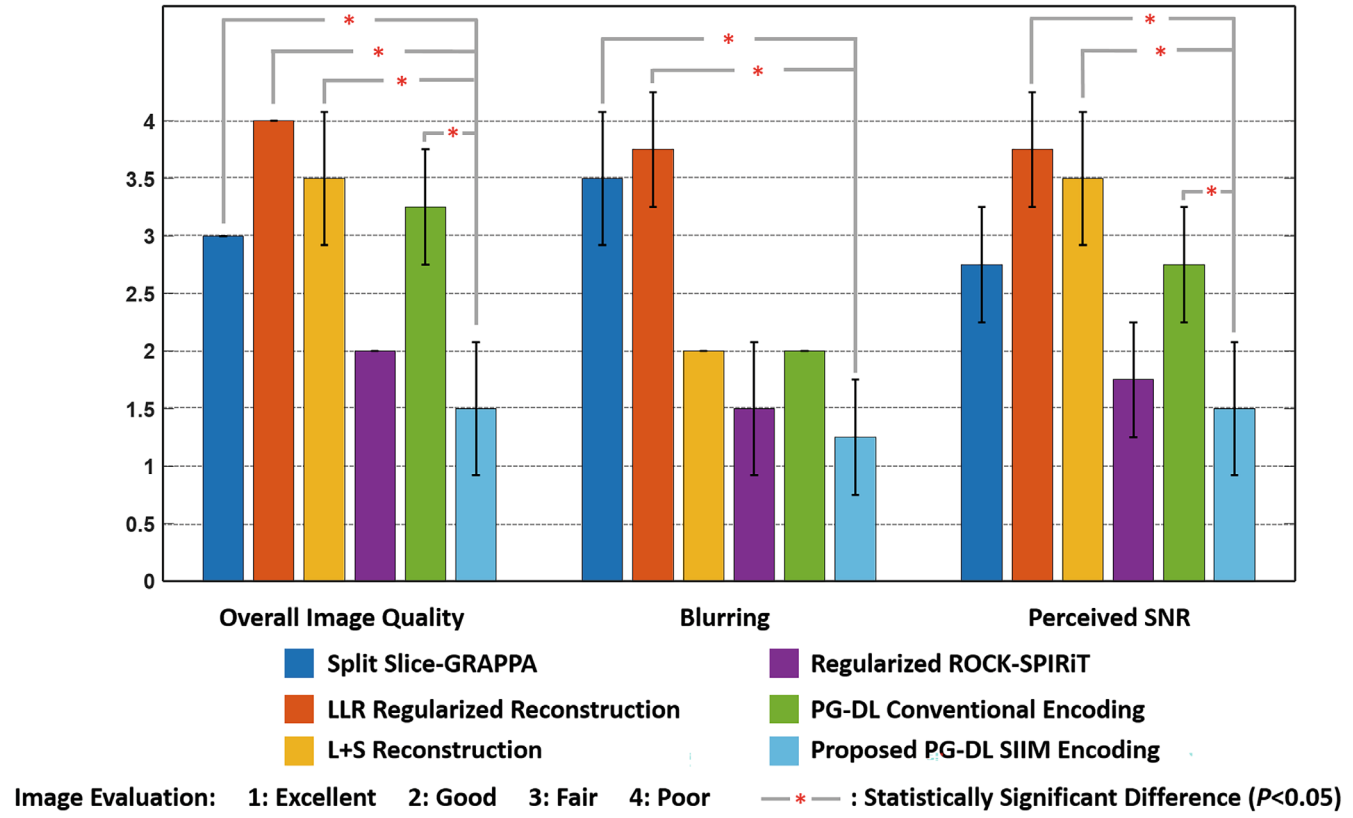

FIGURE 5 The clinical reader study results for the test data sets. Bar plots show average reader scores and their SD across the test subjects for all six reconstruction methods. Statistical testing was performed using Wilcoxon signed-rank test, and * shows significant statistical difference with $P < 0.05$. The proposed PG-DL with SIIM encoding shows the highest overall image quality scores among all methods with significant improvement upon split-slice GRAPPA, LLR-regularized reconstruction, L + S reconstruction and PG-DL with conventional encoding. The proposed method also has the least amount of blurring among all methods, and significantly improves upon split slice-GRAPPA and LLR-regularized reconstruction in terms of blurring. Among all methods, LLR-regularized reconstruction, L + S reconstruction and PG-DL with conventional encoding show the least amount of perceived SNR, whereas the proposed method shows the highest perceived SNR meanwhile significantly improved upon them.

4 | DISCUSSION

In this study, we proposed SIIM encoding operator for PG-DL reconstruction of image series with varying contrast across time-frames, and applied it to highly accelerated myocardial perfusion CMR. The main advantage of using SIIM encoding operator is a uniform/flat signal level across different time-frames at the unrolled neural network output. This in turn facilitates generalizability of PG-DL reconstruction. The proposed approach improved upon multiple regularized reconstructions, showing better image quality, and reduced noise amplification and aliasing.

Conventional and SIIM encoding have two main differences. First, the solution of Eq. [1] using conventional encoding is adversely affected by ill-conditioning at high accelerations.[83] As noted earlier, a similar concept to SIIM encoding was proposed in[74] to improve numerical stability for parallel imaging. The proposed SIIM encoding in Eq. [3] aims for a similar improvement, while enabling a synergistic combination with ESPIRiT, thus not necessitating a different coil map generation process as in.[74] Second, and more importantly, in the PG-DL setup, SIIM encoding provides a more uniform contrast at the neural network outputs across time-frames. The output signal intensity of PG-DL with conventional encoding operator fluctuates across time-frames, and the regularization in the unrolled network needs to work with dramatically different signal levels. On the other hand, SIIM encoding operator maintains a uniform output in terms of signal level. Thus, regularization operates on more uniform SNRs in image space, for the corresponding outputs $\hat{\mathbf{x}}_{\text{SIIM}}$, which empirically generalizes better across time-frames. Even though this intermediate solution has more uniform signal intensity, the final reconstruction is generated by multiplying with the corresponding low-resolution image for that time-frame, restoring the original signal intensity, as indicated in Eq. [2]. Thus, the use of SIIM encoding

operator should not affect quantification in myocardial perfusion, consistent with conclusions from the uptake curves. Finally, on a first look, Eq. [5] may resemble preconditioners in other MRI reconstruction problems,[84–86] which are used to reduce the number of iterations for data fidelity. However, such preconditioners do not change the output signal intensity, thus solution of the preconditioned system coincides with that of the objective in Eq. [1]. Hence, SIIM operator is distinct from this typical use of preconditioning, leading to a more uniform signal intensity across time-frames.

DL reconstruction has gained interest in perfusion CMR, but has been limited to data-driven image enhancement approaches that learn a mapping between aliased and artifact-free images.[66–68] PG-DL approaches, which have been shown to outperform image enhancement methods[62,87,88] have remained elusive for perfusion CMR. One of the main challenges for PG-DL techniques has been related to generalizability with SNR changes,[64] limiting the use of such reconstructions across perfusion time-frames, which is the main issue tackled in this study. Another challenge for DL reconstruction in perfusion CMR has been the lack of gold-standard reference data. Aforementioned data-driven DL methods[66–68] were trained using supervision with compressed sensing reconstructions, limiting the performance of DL reconstruction. On the other hand, PG-DL methods enable self-supervised training from undersampled k-space data only,[61,78,80,89,90] without a reference image. Thus, the combination of SIIM encoding and self-supervised learning for PG-DL, as in this study, has the potential to further improve the utility of DL reconstruction for perfusion CMR.[61] Finally, PG-DL reconstruction can be trained with fewer datasets compared to data-driven DL methods, and the number of k-spaces used for training in this work was in line with earlier PG-DL works that used ~200-to-360 k-spaces,[56–61,64,91,92] and was gathered using only four subjects. We note that the performance gap between the DL methods may change with a substantially larger training database, but this could not be investigated with our current cohort size.

The use of SMS encoding in this study required several design choices related to calibration data. First, since central k-space data were not available for individual slices for each time-frame, an initial split slice-GRAPPA reconstruction was used to generate $\mathbf{L}$, which suppresses aliasing but shows noise amplification. However, since only a limited central k-space region, containing high-SNR low-frequency k-space points, was used to generate $\mathbf{L}$, SNR reduction effects from split slice-GRAPPA were observed to be minimal in subsequent processing. We emphasize that this step was only needed because of SMS encoding, and is not necessary for conventional 2D/3D encoding, where central k-space can be fully-sampled. Furthermore, Blackman filtering was used to avoid ringing, and the reader study did not report any dark rim artifacts associated with the use of $\mathbf{L}$. Second, calibration data for SMS reconstruction were acquired separately in free-breathing, which may be in different respiratory/cardiac motion states than perfusion data. Previously, it was shown that there were no differences between using free-breathing and breath-held calibration in another SMS CMR application in healthy cohorts.[93] Furthermore, ESPIRiT uses only a 24×24 central region, leading to smooth maps, where motion-related artifacts in coil estimation may be non-severe for most cohorts. However, evaluation of these pre-acquired calibration scans warrants further investigation, especially in patient populations with pharmacologically induced stress. Finally, uniform undersampling was used in combination with SMS, since it allows easier integration in clinical sequences, and enables comparisons with clinically-used split slice-GRAPPA reconstruction. We note that compressed sensing methods are often used with random undersampling, thus their performance with uniform undersampling may be deteriorated.

This study has several limitations. All acquisitions in this study were prospectively accelerated. Therefore, there is no gold-standard reference for image quality assessment. Since it is difficult to acquire first-pass perfusion on subjects multiple times due to need for repeated contrast injection, a conventional low-resolution perfusion scan with limited coverage was not performed, excluding a more typical clinical baseline for comparison. Additionally, no stress imaging data were available, which is clinically imperative for perfusion diagnostics. A pixel-wise mapping of myocardial blood flow (MBF) estimation[94] may be performed for quantitative assessment,[95] but such analyses typically require modifications to the imaging protocol, such as administering dual doses[96,97] or using dual sequences.[98–101] Thus, MBF estimation could not be reliably performed with our acquisition protocol. Further clinical studies are warranted to assess full potential of the proposed method, and its diagnostic value in patients with suspected coronary artery disease.

5 | CONCLUSIONS

The proposed PG-DL reconstruction with SIIM encoding operator generalizes well across time-frames/SNRs, and substantially improves upon several existing reconstruction methods for highly accelerated perfusion CMR.

FUNDING INFROMATION

NIH, Grant numbers: R01HL153146, R21EB028369, P41EB027061; NSF, Grant number: CAREER CCF-1651825; NWO Start-Up Grant STU.019.024, 4TU Federation, Health Technology Programme TU Delft - LUMC; AHA Predoctoral Fellowship.

ORCID

Omer Burak Demirel https://orcid.org/0000-0003-4726-0590
Burhaneddin Yaman https://orcid.org/0000-0003-0791-5900
Steen Moeller https://orcid.org/0000-0003-1698-7260
Sebastian Weingärtner https://orcid.org/0000-0002-0739-6306
Mehmet Akçakaya https://orcid.org/0000-0001-6400-7736

REFERENCES

1. Watkins S, McGeoch R, Lyne J, et al. Validation of magnetic resonance myocardial perfusion imaging with fractional flow Reserve for the Detection of significant coronary heart disease. *Circulation*. 2009;120:2207-2213.
2. Eichenberger AC, Schuiki E, Kochli VD, Amann FW, McKinnon GC, Vonschulthess GK. Ischemic heart disease: assessment with gadolinium-enhanced ultrafast MR imaging and dipyridamole stress. *J Magn Reson Imaging*. 1994;4:425-431.
3. Schwitter J, Nanz D, Kneifel S, et al. Assessment of myocardial perfusion in coronary artery disease by magnetic resonance - a comparison with positron emission tomography and coronary angiography. *Circulation*. 2001;103:2230-2235.
4. Ibrahim T, Nekolla SG, Schreiber K, et al. Assessment of coronary flow reserve: comparison between contrast-enhanced magnetic resonance imaging and positron emission tomography. *J Am Coll Cardiol*. 2002;39:864-870.
5. Nagel E, Klein C, Paetsch I, et al. Magnetic resonance perfusion measurements for the noninvasive detection of coronary artery disease. *Circulation*. 2003;108:432-437.
6. Giang TH, Nanz D, Coulden R, et al. Detection of coronary artery disease by magnetic resonance myocardial perfusion imaging with various contrast medium doses: first European multi-Centre experience. *Eur Heart J*. 2004;25:1657-1665.
7. Schwitter J, Wacker CM, van Rossum AC, et al. MR-IMPACT: comparison of perfusion-cardiac magnetic resonance with single-photon emission computed tomography for the detection of coronary artery disease in a multicentre, multivendor, randomized trial. *Eur Heart J*. 2008;29:480-489.
8. Jerosch-Herold M, Wilke N. Cardiovascular Magnetic Resonance 3rd edn. Manning WJ, Pennell DJ; 2019.
9. Coelho OR, Rickers C, Kwong RY, Jerosch-Herold M. MR myocardial perfusion imaging. *Radiology*. 2013;266:701-715.
10. Quinaglia T, Jerosch-Herold M, Coelho-Filho OR. *State-of-the-Art Quantitative Assessment of Myocardial Ischemia by Stress Perfusion Cardiac Magnetic Resonance*. Vol 27. Elsevier; 2019:491-505.
11. Salerno M, Beller GA. Noninvasive assessment of myocardial perfusion. *Circ Cardiovasc Imaging*. 2009;2:412-424.
12. Motwani M, Jogiya R, Kozerke S, Greenwood JP, Plein S. Advanced cardiovascular magnetic resonance myocardial perfusion imaging high-spatial resolution versus 3-dimensional whole-heart coverage. *Circ Cardiovasc Imaging*. 2013;6:339-348.
13. Dewey M, Siebes M, Kachelriess M, et al. Quantitative cardiac imaging S. clinical quantitative cardiac imaging for the assessment of myocardial ischaemia. *Nat Rev Cardiol*. 2020;17:427-450.
14. Pedersen H, Kozerke S, Ringgaard S, Nehrke K, Kim WY. K-t PCA: temporally constrained k-t BLAST reconstruction using principal component analysis. *Magn Reson Med*. 2009;62:706-716.
15. Plein S, Schwitter J, Suerder D, Greenwood JP, Boesiger P, Kozerke S. K-space and time sensitivity encoding-accelerated myocardial perfusion MR imaging at 3.0 T: comparison with 1.5 T. *Radiology*. 2008;249:493-500.
16. Kellman P, Derbyshire JA, Agyeman KO, McVeigh ER, Arai AE. Extended coverage first-pass perfusion imaging using slice-interleaved TSENSE. *Magn Reson Med*. 2004;51:200-204.
17. Salerno M, Sharif B, Arheden H, et al. Recent advances in cardiovascular magnetic resonance techniques and applications. *Circ Cardiovasc Imaging*. 2017;10:e003951.
18. Otazo R, Kim D, Axel L, Sodickson DK. Combination of compressed sensing and parallel imaging for highly accelerated first-pass cardiac perfusion MRI. *Magn Reson Med*. 2010;64:767-776.
19. Naresh NK, Haji-Valizadeh H, Aouad PJ, et al. Accelerated, first-pass cardiac perfusion pulse sequence with radial k-space sampling, compressed sensing, and k-space weighted image contrast reconstruction tailored for visual analysis and quantification of myocardial blood flow. *Magn Reson Med*. 2019;81:2632-2643.
20. Akcakaya M, Basha TA, Pflugi S, et al. Localized Spatio-temporal constraints for accelerated CMR perfusion. *Magn Reson Med*. 2014;72:629-639.
21. Tian Y, Mendes J, Wilson B, et al. Whole-heart, ungated, free-breathing, cardiac-phase-resolved myocardial perfusion MRI by using continuous radial interleaved simultaneous multi-slice acquisitions at sPoiled steady-state (CRIMP). *Magn Reson Med*. 2020;84:3071-3087.
22. Iyer SK, Tasdizen T, Likhite D, DiBella E. Split Bregman multicoil accelerated reconstruction technique: a new framework for rapid reconstruction of cardiac perfusion MRI. *Med Phys*. 2016;43:1969-1981.
23. Wang HN, Adluru G, Chen LY, Kholmovski EG, Bangerter NK, DiBella EVR. Radial simultaneous multi-slice CAIPI for ungated myocardial perfusion. *Magn Reson Imaging*. 2016;34:1329-1336.
24. Sharif B, Arsanjani R, Dharmakumar R, Merz CNB, Berman DS, Li DB. All-systolic non-ECG-gated myocardial perfusion MRI: feasibility of multi-slice continuous first-pass imaging. *Magn Reson Med*. 2015;74:1661-1674.
25. Pflugi S, Roujol S, Akcakaya M, et al. Accelerated cardiac MR stress perfusion with radial sampling after physical exercise with an MR-compatible supine bicycle ergometer. *Magn Reson Med*. 2015;74:384-395.

26. Zhou RX, Huang W, Yang Y, et al. Simple motion correction strategy reduces respiratory-induced motion artifacts for k-t accelerated and compressed-sensing cardiovascular magnetic resonance perfusion imaging. *J Cardiovasc Magn Reson*. 2018;20(1):6.
27. Yang Y, Kramer CM, Shaw PW, Meyer CH, Salerno M. First-pass myocardial perfusion imaging with whole-heart coverage using L1-SPIRiT accelerated variable density spiral trajectories. *Magn Reson Med*. 2016;76:1375-1387.
28. Yang Y, Zhao L, Chen X, et al. Reduced field of view single-shot spiral perfusion imaging. *Magn Reson Med*. 2018;79:208-216.
29. Treutlein C, Wiesmüller M, May MS, et al. Complete free-breathing adenosine stress cardiac MRI using compressed sensing and motion correction: comparison of functional parameters, perfusion, and late enhancement with the standard breath-holding examination. *Radiology*. 2019;1:e180017.
30. Ge L, Kino A, Griswold M, Carr JC, Li DB. Free-breathing myocardial perfusion MRI using SW-CG-HYPR and motion correction. *Magn Reson Med*. 2010;64:1148-1154.
31. Pedersen H, Kelle S, Ringgaard S, et al. Quantification of myocardial perfusion using free-breathing MRI and prospective slice tracking. *Magn Reson Med*. 2009;61:734-738.
32. Cleppien DEJ, Horstick G, Abegunewardene N, et al. Comparison of the quantitative first pass myocardial perfusion MRI with and without prospective slice tracking: comparison between breath-hold and free-breathing condition. *Magn Reson Med*. 2010;64:1462-1471.
33. Otazo R, Kim D, Axel L, Sodickson D. Combination of compressed sensing and parallel imaging with respiratory motion correction for highly-accelerated cardiac perfusion MRI. Volume 13. *J Cardiovasc Magn Reson*. 2011;13:98.
34. Miao X, Lingala SG, Guo Y, et al. Accelerated cardiac cine MRI using locally low rank and finite difference constraints. *Magn Reson Imaging*. 2016;34:707-714.
35. Otazo R, Candes E, Sodickson DK. Low-rank plus sparse matrix decomposition for accelerated dynamic MRI with separation of background and dynamic components. *Magn Reson Med*. 2015;73:1125-1136.
36. Liu F, Li DX, Jin XY, Qiu WY, Xia Q, Sun B. Dynamic cardiac MRI reconstruction using motion aligned locally low rank tensor (MALLRT). *Magn Reson Imaging*. 2020;66:104-115.
37. Lin CY, Fessler JA. Efficient dynamic parallel MRI reconstruction for the low-rank plus sparse model. *IEEE Trans Comput Imaging*. 2019;5:17-26.
38. Wang D, Smith DS, Yang XP. Dynamic MR image reconstruction based on total generalized variation and low-rank decomposition. *Magn Reson Med*. 2020;83:2064-2076.
39. Arif O, Afzal H, Abbas H, Amjad MF, Wan JF, Nawaz R. Accelerated dynamic MRI using kernel-based low rank constraint. *J Med Syst*. 2019;43:271.
40. Yao JW, Xu Z, Huang XL, Huang JZ. An efficient algorithm for dynamic MRI using low-rank and total variation regularizations. *Med Image Anal*. 2018;44:14-27.
41. Shin T, Hu HH, Pohost GM, Nayak KS. Three dimensional first-pass myocardial perfusion imaging at 3T: feasibility study. *J Cardiovasc Magn Reson*. 2008;10(1):57.
42. Manka R, Wissmann L, Gebker R, et al. Multicenter evaluation of dynamic three-dimensional magnetic resonance myocardial perfusion imaging for the detection of coronary artery disease defined by fractional flow reserve. *Circ Cardiovasc Imaging*. 2015;8:e003061.
43. Jogiya R, Schuster A, Zaman A, et al. Three-dimensional balanced steady state free precession myocardial perfusion cardiovascular magnetic resonance at 3T using dual-source parallel RF transmission: initial experience. *J Cardiovasc Magn Reson*. 2014;16:1-10.
44. Manka R, Jahnke C, Kozerke S, et al. Dynamic 3-dimensional stress cardiac magnetic resonance perfusion imaging detection of coronary artery disease and Volumetry of myocardial Hypoenhancement before and after coronary stenting. *J Am Coll Cardiol*. 2011;57:437-444.
45. Vitanis V, Manka R, Giese D, et al. High resolution three-dimensional cardiac perfusion imaging using compartment-based k-t principal component analysis. *Magn Reson Med*. 2011;65:575-587.
46. Wang HN, Bangerter NK, Park DJ, et al. Comparison of centric and reverse-centric trajectories for highly accelerated three-dimensional saturation recovery cardiac perfusion imaging. *Magn Reson Med*. 2015;74:1070-1076.
47. Giri S, Xue H, Maiseyeu A, et al. Steady-state first-pass perfusion (SSFPP): a new approach to 3D first-pass myocardial perfusion imaging. *Magn Reson Med*. 2014;71:133-144.
48. Shin T, Nayak KS, Santos JM, Nishimura DG, Hu BS, McConnell MV. Three-dimensional first-pass myocardial perfusion MRI using a stack-of-spirals acquisition. *Magn Reson Med*. 2013;69:839-844.
49. Vitanis V, Manka R, Boesiger P, Kozerke S, IEEE. High Resolution 3D Cardiac Perfusion Imaging Using Compartment-Based k-t PCA. IEEE Engineering in Medicine and Biology Society Conference Proceedings, Buenos Aires, Argentina. 2010:21–24.
50. Nazir MS, Shome J, Villa ADM, et al. 2D high resolution vs. 3D whole heart myocardial perfusion cardiovascular magnetic resonance. Volume 00. *Eur Heart J Cardiovasc Imaging*. 2021;23:1-9.
51. Nazir MS, Neji R, Speier P, et al. Simultaneous multi slice (SMS) balanced steady state free precession first-pass myocardial perfusion cardiovascular magnetic resonance with iterative reconstruction at 1.5T. *J Cardiovasc Magn Reson*. 2018;20:1-11.
52. Yang Y, Meyer CH, Epstein FH, Kramer CM, Salerno M. Whole-heart spiral simultaneous multi-slice first-pass myocardial perfusion imaging. *Magn Reson Med*. 2019;81:852-862.
53. McElroy S, Ferrazzi G, Nazir MS, et al. Combined simultaneous multislice bSSFP and compressed sensing for first-pass myocardial perfusion at 1.5 T with high spatial resolution and coverage. *Magn Reson Med*. 2020;84:3103-3116.
54. Wang JY, Yang Y, Weller DS, et al. High spatial resolution spiral first-pass myocardial perfusion imaging with whole-heart coverage at 3 T. *Magn Reson Med*. 2021;86:648-662.
55. Weingärtner S, Moeller S, Akcakaya M. Feasibility of ultra-high simultaneous multi-slice and in-plane accelerations for cardiac MRI using outer volume suppression and leakage-blocking reconstruction. Annual Meeting of the International Society of Magnetic Resonance in Medicine, 2018:0359.
56. Hammernik K, Klatzer T, Kobler E, et al. Learning a variational network for reconstruction of accelerated MRI data. *Magn Reson Med*. 2018;79:3055-3071.

57. Aggarwal HK, Mani MP, Jacob M. MoDL: model-based deep learning architecture for inverse problems. *IEEE Trans Med Imaging*. 2019;38:394-405.
58. Schlemper J, Caballero J, Hajnal JV, Price AN, Rueckert D. A deep Cascade of convolutional neural networks for dynamic MR image reconstruction. *IEEE Trans Med Imaging*. 2018;37:491-503.
59. Qin C, Schlemper J, Caballero J, Price AN, Hajnal JV, Rueckert D. Convolutional recurrent neural networks for dynamic MR image reconstruction. *IEEE Trans Med Imaging*. 2019;38:280-290.
60. Hosseini SAH, Yaman B, Moeller S, Hong MY, Akcakaya M. Dense recurrent neural networks for accelerated MRI: history-Cognizant unrolling of optimization algorithms. *IEEE J Selected Topics Signal Process*. 2020;14:1280-1291.
61. Yaman B, Hosseini SAH, Moeller S, Ellermann J, Ugurbil K, Akcakaya M. Self-supervised learning of physics-guided reconstruction neural networks without fully sampled reference data. *Magn Reson Med*. 2020;84:3172-3191.
62. Knoll F, Hammernik K, Zhang C, et al. Deep-learning methods for parallel magnetic resonance imaging reconstruction: a survey of the current approaches, trends, and issues. *IEEE Signal Process Mag*. 2020;37:128-140.
63. Akçakaya M, Yaman B, Chung H, Ye JC. Unsupervised deep learning methods for biological image reconstruction and enhancement. *IEEE Signal Process Mag*. 2022;39:28-44.
64. Knoll F, Hammernik K, Kobler E, Pock T, Recht MP, Sodickson DK. Assessment of the generalization of learned image reconstruction and the potential for transfer learning. *Magn Reson Med*. 2019;81:116-128.
65. Kofler A, Dewey M, Schaeffter T, Wald C, Kolbitsch C. Spatio-temporal deep learning-based Undersampling artefact reduction for 2D radial cine MRI with limited training data. *IEEE Trans Med Imaging*. 2020;39:703-717.
66. Fan LXZ, Shen DM, Haji-Valizadeh H, et al. Rapid dealiasing of undersampled, non-Cartesian cardiac perfusion images using U-net. *NMR Biomed*. 2020;33:e4239.
67. Le J, Tian Y, Mendes J, et al. Deep learning for radial SMS myocardial perfusion reconstruction using the 3D residual booster U-net. *Magn Reson Imaging*. 2021;83:178-188.
68. Wang JY, Weller DS, Kramer CM, Salerno M. DEep learning-based rapid spiral image REconstruction (DESIRE) for high-resolution spiral first-pass myocardial perfusion imaging. *NMR Biomed*. 2022;35:e4661.
69. Cauley SF, Polimeni JR, Bhat H, Wald LL, Setsompop K. Interslice leakage artifact reduction technique for simultaneous multislice acquisitions. *Magn Reson Med*. 2014;72:93-102.
70. Zhang T, Pauly JM, Levesque IR. Accelerating parameter mapping with a locally low rank constraint. *Magn Reson Med*. 2015;73:655-661.
71. Demirel OB, Weingartner S, Moeller S, Akcakaya M. Improved simultaneous multislice cardiac MRI using readout concatenated k-space SPIRiT (ROCK-SPIRiT). *Magn Reson Med*. 2021;85:3036-3048.
72. Fessler JA. Optimization methods for magnetic resonance image reconstruction: key models and optimization algorithms. *IEEE Signal Process Mag*. 2020;37:33-40.
73. Uecker M, Lai P, Murphy MJ, et al. ESPIRiT-an eigenvalue approach to autocalibrating parallel MRI: where SENSE meets GRAPPA. *Magn Reson Med*. 2014;71:990-1001.
74. Sodickson DK, McKenzie CA. A generalized approach to parallel magnetic resonance imaging. *Med Phys*. 2001;28:1629-1643.
75. Breuer FA, Blaimer M, Heidemann RM, Mueller MF, Griswold MA, Jakob PM. Controlled aliasing in parallel imaging results in higher acceleration (CAIPIRINHA) for multi-slice imaging. *Magn Reson Med*. 2005;53:684-691.
76. Veraart J, Fieremans E, Jelescu IO, Knoll F, Novikov DS. Gibbs ringing in diffusion MRI. *Magn Reson Med*. 2016;76:301-314.
77. Pruessmann KP, Weiger M, Scheidegger MB, Boesiger P. SENSE: sensitivity encoding for fast MRI. *Magn Reson Med*. 1999;42:952-962.
78. Yaman B, Shenoy C, Deng Z, Moeller S, El-Rewaidy H, Nezafat R, Akcakaya M. Self-supervised physics-guided deep learning reconstruction for high-resolution 3D LGE CMR. IEEE 18th International Symposium on Biomedical Imaging (ISBI), 2021:100–104.
79. Yaman B, Hosseini SAH, Moeller S, Ellermann J, Ukurbil K, Akcakaya M, IEEE. Self-supervised physics-based deep learning mri reconstruction without fully-sampled data. 2020 IEEE17th International Symposium on Biomedical Imaging (ISBI 2020), 2020:921–925.
80. Yaman B, Hosseini SAH, Moeller S, Ellermann J, Ugurbil K, Akcakaya M. Multi-mask self-supervised learning for physics-guided neural networks in highly accelerated magnetic resonance imaging. *NMR Biomed*. 2022 Jul;5:e4798. doi:10.1002/nbm.4798
81. Wissmann L, Santelli C, Segars WP, Kozerke S. MRXCAT: realistic numerical phantoms for cardiovascular magnetic resonance. *J Cardiovasc Magn Reson*. 2014;16:1-11.
82. Zarinabad N, Chiribiri A, Hautvast G, Breeuwer M, Nagel E. Influence of spatial resolution on the accuracy of quantitative myocardial perfusion in first pass stress perfusion CMR. *Magn Reson Med*. 2015;73:1623-1631.
83. Doneva M. Mathematical models for magnetic resonance imaging reconstruction: an overview of the approaches, problems, and future research areas. *IEEE Signal Process Mag*. 2020;37:24-32.
84. Pruessmann KP, Weiger M, Bornert P, Boesiger P. Advances in sensitivity encoding with arbitrary k-space trajectories. *Magn Reson Med*. 2001;46:638-651.
85. Koolstra K, van Gemert J, Bornert P, Webb A, Remis R. Accelerating compressed sensing in parallel imaging reconstructions using an efficient circulant preconditioner for cartesian trajectories. *Magn Reson Med*. 2019;81:670-685.
86. Baron CA, Dwork N, Pauly JM, Nishimura DG. Rapid compressed sensing reconstruction of 3D non-Cartesian MRI. *Magn Reson Med*. 2018;79:2685-2692.
87. Muckley MJ, Riemenschneider B, Radmanesh A, et al. Results of the 2020 fastMRI challenge for machine learning MR image reconstruction. *IEEE Trans Med Imaging*. 2021;40:2306-2317.
88. Knoll F, Murrell T, Sriram A, et al. Advancing machine learning for MR image reconstruction with an open competition: overview of the 2019 fastMRI challenge. *Magn Reson Med*. 2020;84:3054-3070.
89. Demirel OB, Yaman B, Dowdle L, Moeller S, Vizioli L, Yacoub E, Strupp J, Olman CA, Ugurbil K, Akcakaya M. Improved simultaneous multi-slice functional MRI using self-supervised deep learning. 55th Asilomar Conference on Signals, Systems, and Computers. IEEE, 2021; 890–894.

90. Demirel OB, Yaman B, Dowdle L, Moeller S, Vizioli L, Yacoub E, Strupp J, Olman CA, Ugurbil K, Akcakaya M, IEEE. 20-fold accelerated 7T fMRI using Referenceless self-supervised deep learning reconstruction. 43rd Annual International Conference of the IEEE Engineering in Medicine & Biology Society (EMBC). IEEE, 2021:3765–3769.
91. Duan JM, Schlemper J, Qin C, Ouyang C, Bai WJ, Biffi C, Bello G, Statton B, O'Regan DP, Rueckert D. VS-net: variable splitting network for accelerated parallel MRI reconstruction. Medical image computing and computer assisted intervention - Miccai 2019, Pt Iv 2019;11767:713–722.
92. Kellman M, Zhang K, Markley E, et al. Memory-efficient learning for large-scale computational imaging. *IEEE Trans Comput Imaging*. 2020;6:1403-1414.
93. Weingartner S, Moeller S, Schmitter S, et al. Simultaneous multislice imaging for native myocardial T-1 mapping: improved spatial coverage in a single breath-hold. *Magn Reson Med*. 2017;78:462-471.
94. Heydari B, Kwong RY, Jerosch-Herold M. Technical advances and clinical applications of quantitative myocardial blood flow imaging with cardiac MRI. *Prog Cardiovasc Dis*. 2015;57:615-622.
95. Camici PG, Rimoldi OE. The clinical value of myocardial blood flow measurement. *J Nucl Med*. 2009;50:1076-1087.
96. Christian TF, Aletras AH, Arai AE. Estimation of absolute myocardial blood flow during first-pass MR perfusion imaging using a dual-bolus injection technique: comparison to single-bolus injection method. *J Magn Reson Imaging*. 2008;27:1271-1277.
97. Hsu LY, Rhoads KL, Holly JE, Kellman P, Aletras AH, Arai AE. Quantitative myocardial perfusion analysis with a dual-bolus contrast-enhanced first-pass MRI technique in humans. *J Magn Reson Imaging*. 2006;23:315-322.
98. Gatehouse PD, Elkington AG, Ablitt NA, Yang GZ, Pennell DJ, Firmin DN. Accurate assessment of the arterial input function during high-dose myocardial perfusion cardiovascular magnetic resonance. *J Magn Reson Imaging*. 2004;20:39-45.
99. Hsu LY, Jacobs M, Benovoy M, et al. Diagnostic performance of fully automated pixel-wise quantitative myocardial perfusion imaging by cardiovascular magnetic resonance. *JACC Cardiovasc Imaging*. 2018;11:697-707.
100. Kellman P, Hansen MS, Nielles-Vallespin S, et al. Myocardial perfusion cardiovascular magnetic resonance: optimized dual sequence and reconstruction for quantification. *J Cardiovasc Magn Reson*. 2017;19:43.
101. Hoh T, Vishnevskiy V, Polacin M, Manka R, Fuetterer M, Kozerke S. Free-breathing motion-informed locally low-rank quantitative 3D myocardial perfusion imaging. *Magn Reson Med*. 2022;88:1575-1591.

SUPPORTING INFORMATION

Additional supporting information may be found in the online version of the article at the publisher's website.

Video S1. Movie of the perfusion images reconstructed with all techniques of a test subject (shown in Figure 2).

Video S2. Movie of the perfusion images reconstructed with all techniques of another test subject.

Figure S1. Details of variable splitting for solving the inverse problem.

Figure S2. Details of implementation for SMS encoding (A) SMS forward model for the acquisition where $y_{\Omega}^{\mathrm{SMS}}$ is the acquired multi-channel SMS k-space, $E_{\Omega}^{[i]}$ is the multi-coil encoding operator of the ith slice, $x^{[i]}$ is the underlying image corresponding to the i$^{\mathrm{th}}$ simultaneously excited slice, and n_{slice} is the number of SMS-excited slices. (B) The notation in (A) can be condensed by concatenating simultaneously excited slices, $\left\{x^{[i]}\right\}_{\mathrm{i}=1}^{n_{\mathrm{slice}}}$, along the readout direction, as x^{SMS} which yields a compact form of multi-coil and multi-slice operator $E_{\Omega}^{\mathrm{SMS}} = \left[E_{\Omega}^{[1]} \ \cdots \ E_{\Omega}^{\left[n_{\mathrm{slice}}\right]}\right]$.[5–7] (C) For the SIIM encoding operator, we let L_{SMS} be a block diagonal matrix whose entries are also diagonal matrices, $L_{[i]}$ that encode the signal variations in the ith SMS-excited slice, such as a low-resolution image, defined as L_{SMS}. Note that, as before, for ease of notation, we simply use $L_{[i]}$, but there are $T \cdot n_{\mathrm{slice}}$ different low-resolution images with $L_{[i]}^{t}, t \in \{1, \cdots, T\}, i \in \{1, \cdots, n_{\mathrm{slice}}\}$, when different time-frames are considered. Finally, SIIM encoding operator for SMS imaging is given as $H_{\Omega}^{\mathrm{SMS}} = E_{\Omega}^{\mathrm{SMS}} L_{\mathrm{SMS}}$

Figure S3. Details of self-supervised deep learning implementation

Figure S4. (A) The ResNet structure consisted of 15 residual blocks with skip connections which were used to facilitate the information flow during training and each block has two convolutional layers.[11] (A) The ResNet structure consisted of 15 residual blocks with skip connections which were used to facilitate the information flow during training and each block has two convolutional layers.[9] (B) First layer of the residual block was followed by a rectified linear unit (ReLU) and the latter was followed by a constant multiplication corresponding to 0.1.[9] All layers in the network had kernel size of 3×3 and 64 channels, for a total of 592 129 trainable parameters which were shared across unrolled iterations. The three SMS slices were concatenated along the readout direction prior to being input to the ResNet with proper FOV shifts to reorient the CAIPIRINHA phase cycling and avoid boundary artifacts.[5,6]

Figure S5. Representative numerical phantom results for myocardial perfusion CMR simulated with a 3-fold SMS and 4-fold in-plane acceleration along with outer volume suppression.

Figure S6. The error images between full-sampled reference images and all reconstruction methods for the numerical phantom experiments.

Figure S7. Signal intensity plots of left ventricular contrast uptake and 6 AHA segments of myocardial contrast uptake for all methods.

Figure S8. Difference images between split slice-GRAPPA and all the regularized reconstruction methods.

Figure S9. All 9 slices for a representative time-frame, covering the whole heart using 3 SMS groups of 9 slices from another subject shown in Figure 3.

Figure S10. Low-pass filtered signal intensity curves of hand-drawn 6 AHA sectors in myocardium.

Table S1. Free-breathing first-pass myocardial perfusion CMR imaging sequence details.[4]

Table S2. Implementation details of the PG-DL networks used in this study.

Table S3. Implementation details of comparison reconstruction methods. All thresholding values were empirically tuned to maximize visual image quality.

Table S4. Implementation details of the numerical phantom.

Table S5. Image quality assessment scores using PSNR and SSIM for all reconstruction methods using the numerical phantom.

How to cite this article: Demirel OB, Yaman B, Shenoy C, Moeller S, Weingärtner S, Akçakaya M. Signal intensity informed multi-coil encoding operator for physics-guided deep learning reconstruction of highly accelerated myocardial perfusion CMR. *Magn Reson Med*. 2022;1-14. doi: 10.1002/mrm.29453